New Constraints on Dark Photon Dark Matter with Superconducting Nanowire Detectors in an Optical Haloscope

Jeff Chiles,[1,*,‡] Ilya Charaev,[2,3,†,‡] Robert Lasenby,[4] Masha Baryakhtar,[5] Junwu Huang,[6] Alexana Roshko,[1] George Burton,[1] Marco Colangelo,[2] Ken Van Tilburg,[7,8] Asimina Arvanitaki,[6] Sae Woo Nam,[1] and Karl K. Berggren[2]

[1]*National Institute of Standards and Technology, 325 Broadway, Boulder, Colorado 80305, USA*
[2]*Massachusetts Institute of Technology, 50 Vassar Street, Cambridge, Massachusetts 02139, USA*
[3]*University of Zurich, Zurich 8057, Switzerland*
[4]*Stanford Institute for Theoretical Physics, Stanford University, Stanford, California 94305, USA*
[5]*Department of Physics, University of Washington, Seattle, Washington 98195, USA*
[6]*Perimeter Institute for Theoretical Physics, Waterloo, Ontario N2L 2Y5, Canada*
[7]*New York University CCPP, New York, New York 10003, United States*
[8]*Center for Computational Astrophysics, Flatiron Institute, New York, New York 10010, USA*

(Received 22 October 2021; revised 29 April 2022; accepted 13 May 2022; published 10 June 2022; corrected 29 September 2022 and 22 December 2022)

Uncovering the nature of dark matter is one of the most important goals of particle physics. Light bosonic particles, such as the dark photon, are well-motivated candidates: they are generally long-lived, weakly interacting, and naturally produced in the early universe. In this work, we report on Light A' Multilayer Periodic Optical SNSPD Target, a proof-of-concept experiment searching for dark photon dark matter in the eV mass range, via coherent absorption in a multilayer dielectric haloscope. Using a superconducting nanowire single-photon detector (SNSPD), we achieve efficient photon detection with a dark count rate of $\sim 6 \times 10^{-6}$ counts/s. We find no evidence for dark photon dark matter in the mass range of ~0.7–0.8 eV with kinetic mixing $\epsilon \gtrsim 10^{-12}$, improving existing limits in ϵ by up to a factor of 2. With future improvements to SNSPDs, our architecture could probe significant new parameter space for dark photon and axion dark matter in the meV to 10 eV mass range.

DOI: 10.1103/PhysRevLett.128.231802

Dark matter (DM), a form of nonrelativistic matter that amounts to ~25% of the energy budget of the universe [1,2], is by now the conservative explanation for a wealth of astrophysical and cosmological data that cannot be accommodated within the standard model (SM) of particle physics. However, all of our evidence for DM is via its gravitational interactions on large scales, which is compatible with a very wide range of particle physics models.

Light, weakly coupled new bosons are a well-motivated class of DM candidates [3–7]. Light scalar, pseudoscalar, and vector particles arise in many SM extensions and are generally weakly coupled, long-lived, and difficult to detect [8–13]. These bosonic DM candidates are also automatically produced in the early universe assuming a period of cosmic inflation [5,7]. For vector DM, the abundance today depends on the inflationary Hubble scale [7], and can yield the measured DM abundance for DM masses $\gtrsim 5 \times 10^{-5}$ eV given current constraints on the inflationary scale [14]. The detection of a vector DM particle at the eV scale would point to a Hubble scale of 5×10^{12} GeV, otherwise unreachable in any laboratory experiment or late-universe astrophysical observation.

The simplest and least-constrained vector DM model is the dark photon, characterized by the "kinetic mixing" interaction with the photon [10]

$$\mathcal{L} \supset -\frac{1}{4}F_{\mu\nu}F^{\mu\nu} - \frac{1}{4}F'_{\mu\nu}F'^{\mu\nu} - \frac{1}{2}\epsilon F_{\mu\nu}F'^{\mu\nu} + \frac{1}{2}m_{A'}^2 A'^2, \quad (1)$$

where $F_{\mu\nu}$ and $F'_{\mu\nu}$ are the field strengths of the photon and the dark photon, respectively, and A' is the dark photon field. The dark photon mass $m_{A'}$ and kinetic mixing parameter $\epsilon \ll 1$ define the DM parameter space.

Similarly to a photon, the leading interaction between dark photon DM and a detector is the *absorption* of the DM particle [15,16]. The entire rest mass energy $m_{A'}c^2$ can be captured, in contrast to scattering, which deposits at most the kinetic energy $m_{A'}v^2/2$ in direct detection experiments [17] (where $v \sim 10^{-3}c$ is the galactic DM velocity and c is the speed of light). This motivates new experimental schemes for the detection of light bosonic DM. In this

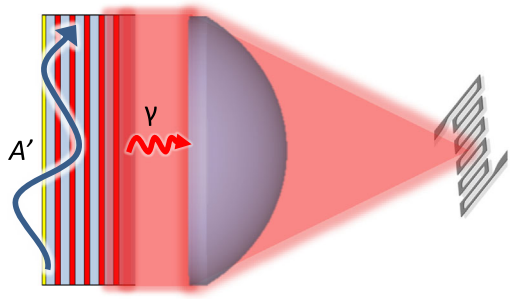

FIG. 1. Sketch of the LAMPOST concept. The dark photon dark matter field A' converts to photons in a layered dielectric target. These photons are focused by a lens onto a small, low-noise SNSPD detector. The beam emitted from the stack is approximately uniform except for a small region in the middle where a mirror is absent, not shown here.

Letter, we focus on the efficient conversion of dark photon DM to near-IR photons.

To convert a nonrelativistic dark photon into a relativistic photon of the same frequency, the target must compensate for the mismatch in momentum. This can be achieved using a stack of dielectric layers with different indices of refraction, whose thicknesses are on the scale of the photon's wavelength [15,18–21]; we use a stack of half-wavelength layers [22]. In such a structure, dark photon DM at the corresponding frequency can convert coherently to photons: the photon acquires its energy from the dark photon DM and its momentum from the lattice vector of the photonic crystal, thus alleviating the momentum mismatch between the nonrelativistic DM and the relativistic photon (see Fig. 1 for a sketch of the setup). In particular, in a half wave stack [22], due to constructive interference between converted photons from different layers, the conversion rate increases as the square of the number of layer periods N. If the half wave frequency is matched to the DM mass, then the converted power per unit area is given by

$$\frac{P}{A} \simeq \frac{8}{3}\epsilon^2 \rho_{\mathrm{DM}} N^2 \left(\frac{1}{n_1^2} - \frac{1}{n_2^2}\right)^2, \tag{2}$$

where $\rho_{\mathrm{DM}} \simeq 0.4\ \mathrm{GeV\,cm^{-3}}$ is the local DM density, $n_{1,2}$ are the refractive indices of the alternating layers, and A is the area of the stack (Fig. 3 shows the converted power as a function of DM mass for our stack configuration).

Due to the small DM velocity, the converted photons are emitted within $\sim 10^{-3}$ rad of the normal vector to the layers. This allows them to be focused down to an area $\sim 10^{-6}$ smaller than that of the layers, permitting the use of small, highly sensitive detectors [15,16,18]. Superconducting nanowire single-photon detectors (SNSPDs) have demonstrated, in separate experiments, ultralow dark count rates (10^{-6} Hz) necessary to detect rare signal events, active areas large enough to collect the focused light ($\gtrsim 0.1\ \mathrm{mm^2}$), near-unity detection efficiency, and sensitivity to photons from 0.1 eV to 10 eV [23–26]. These properties make SNSPDs well suited to the unique requirements of this project.

In this Letter, we present the first results from the LAMPOST (Light A' Multilayer Periodic Optical SNSPD Target) experiment with 180 hours of data collection. Our simple and inexpensive prototype constrains new dark photon DM parameter space at masses ~0.7–0.8 eV (corresponding to photon wavelengths ~1550–1770 nm) with less than a week of run time. The choice of the ~0.7–0.8 eV mass range allows us to leverage off-the-shelf equipment and robust fabrication processes to simplify this proof-of-concept experiment.

Experimental setup.—The dielectric stack, or target, generates the signal photons of interest. As discussed in Ref. [15], a useful configuration is a "half wave" stack, in which the stack's layers have alternating refractive indices $n_1, n_2, n_1, n_2, \ldots$ and thicknesses $d_1, d_2, d_1, d_2, \ldots$, with $n_1 d_1 = n_2 d_2$. The thicknesses and indices are chosen for light at the signal wavelength of interest to acquire π phase upon transmitting through each layer. In such a material, dark photon DM with frequency $\omega \simeq \pi / n_i d_i$ can convert coherently to photons. We utilize alternating layers of amorphous silicon and silica, deposited on top of a ~0.525 mm thick silica substrate which is polished on both sides.

The dielectric stack is integrated and aligned with several optomechanical elements and a 50 mm focal length plano-convex lens to focus the signal onto the primary SNSPD. The structure is illustrated in the right-hand panel of Fig. 2. A reference SNSPD, nominally identical to the first, is placed on the same printed circuit board (PCB) as the primary detector, but offset by 2 cm so as to be completely

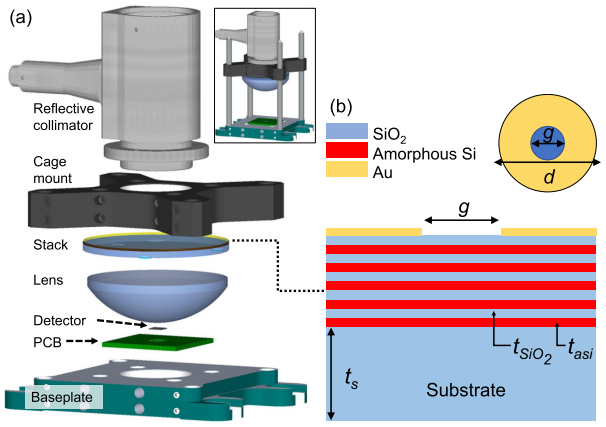

FIG. 2. The LAMPOST prototype haloscope apparatus. (a) Exploded view with element details. Inset: assembled view. (b) Schematic cross-sectional and top views of the dielectric stack target responsible for DM-signal photon conversion, with designed values of different dimensions, g, aperture diameter, 10 mm; d, wafer diameter, 50 mm; t_s, substrate thickness, 525 μm; t_{asi}, amorphous silicon layer thickness, ~292 nm; t_s, SiO_2 layer thickness, ~548 nm. See the Supplemental Material [28] for details of the film characterization.

out of the optical path of the signal. This reference detector can serve to provide an estimate of the event rate for several potential sources of background counts, including cosmic ray muons, Cherenkov photons generated in the lens [27], or high energy particles excited by radioactive decay events. The entire apparatus is contained inside a light-tight box.

To electrically and optically characterize the fabricated SNSPDs, we designed an experimental setup using a sorption-pump type He-3 cryostat. The haloscope containing the SNSPDs (the assembly in Fig. 2) was placed on a 300 mK cold stage, with ample spacing from the innermost radiation shield. The signal was amplified at the 4 K stage by a cryogenic low-noise amplifier with a total gain of 56 dB and then was sent to a pulse counter. A single mode optical fiber delivered light from 1550 nm and 1700 nm CW lasers into the cryogenic apparatus though a vacuum feedthrough.

An important consideration is whether the apparatus is mechanically stable enough to preserve the intended alignment during the cooldown. A mock haloscope was constructed to independently test this (which used the same SNSPD and PCB). We can detect a misalignment by comparing the experimental and theoretical detection efficiency (DE) of the SNSPD; a large discrepancy would suggest substantial misalignment. First, we placed a conventional, large-area optical power meter directly above the SNSPD at room temperature and recorded the optical power at a fixed laser power output at 1550 nm. Next, we removed the power meter, cooled the system to 300 mK, and recorded the photon count rate on the SNSPD for the same laser output power (but with a fixed and known optical attenuation added to the signal path to avoid saturating the SNSPD). A DE of $28.3 \pm 0.5\%$ was observed for the case of light polarized along the length of the wire (parallel) and $12.1 \pm 0.5\%$ for the perpendicular polarization. A paddle-type polarization controller was used to shift the state as needed. We simulated the theoretical DE of our detector to be 33.6% for the parallel polarization case and 10.6% for the perpendicular case (described further in the next section). We note that the experimental parallel DE of $28.3 \pm 0.5\%$ could be 1.117 times higher, or 31.6%, if the SNSPD were operated at a higher bias current (this is necessary to facilitate direct comparison to the simulations, where the internal detection efficiency is assumed to be unity). Comparing the experimental DE of 31.6% (after compensating for incomplete saturation of the internal detection efficiency) to the simulated DE of 33.6% for the parallel polarization case, the magnitude differs only by a factor of 0.94. The discrepancy may be explained by small temporal variations in laser source power (∼2%), incomplete polarization state purity (∼1–2%), variable scattering loss at fiber connectors at different temperatures, and an acceptable amount of misalignment in the beam. The larger-than-expected perpendicular polarization DE and smaller-than-expected parallel DE would be consistent with a slightly impure polarization state during the measurement. We note that the targeting beam changed position by 100 μm in both the lateral directions upon warming up after this mock haloscope test, which was consistent with the behavior of the main haloscope during the actual experiment.

Separately, the main haloscope was assembled and tested briefly prior to the data collection. A brief optical measurement at cryogenic temperatures was conducted (without control over polarization), giving a reasonable DE of 19.3% which is between the nominal parallel and perpendicular DE values. Next, the system was warmed to room temperature, and the optical fiber was disconnected to prevent blackbody radiation-induced counts impinging on the detector. After cooling down again, we began recording counts on the main detector over several cycles of the cryostat. At several points, the haloscope was removed from the system, and the optical alignment was inspected to ensure no significant drift had occurred. A translational drift of about 100 μm was observed, consistent with the detailed alignment test conducted separately. We collected count data for both the main and reference SNSPDs over a total time of 180 hours at the 300 mK base temperature, while operating both SNSPDs at a bias current of 4.2 μA.

After assembling the dielectric stack and the SNSPD as in Fig. 2, we combine simulated and experimentally measured factors to obtain a well-bounded number for the system detection efficiency (SDE), which captures all known sources of loss from the point of signal photon generation in the stack to the generation of photon count events in the SNSPD. The SDE can be expressed as

$$\mathrm{SDE} = \mathrm{OCE} \times T \times \mathrm{DE}. \tag{3}$$

The optical collection efficiency (OCE) is derived from ray-tracing simulations as described in the Supplemental Material [28]. The simulations show that 1.27% of signal photons generated in the stack impinge on the SNSPD in the worst-case misalignment. The OCE constitutes the largest source of loss in our system, and is limited by several factors, including a ± 100 μm in plane alignment uncertainty (experimentally observed), spherical aberration, and total internal reflection losses in the lens. Additionally, we found that wafer curvature resulting from intrinsic stress in the dielectric stack's thin films modified the focal length from the expected value, further misaligning the signal (see Supplemental Material [28]). The transmission coefficient $T = 88\%$ captures a small optical loss incurred by defects in the dielectric stack which scatter the signal. Finally, the DE of the SNSPD is the probability of generating a detection event for one photon incident on the detector's footprint; the value is estimated to be 17.5% based on a calibrated measurement of the DE at 1550 nm, which is averaged for both polarization states, followed by

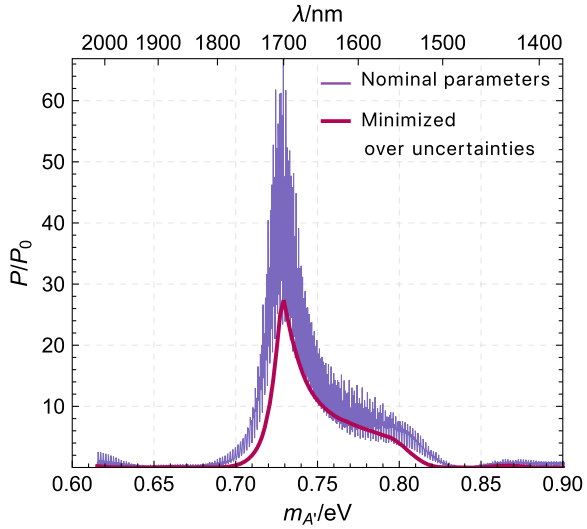

FIG. 3. Calculated time-averaged power P absorbed from dark photon DM with mass $m_{A'}$ by the layered target, normalized to the power P_0 absorbed by a uniform mirror. The thin purple curve shows the power absorbed by a target with parameters given by their respective measured central values, while the magenta curve shows the minimum power obtained by varying the parameters within measurement uncertainties (see the Supplemental Material [28]). The substrate thickness is assumed to physically vary by $\gtrsim$10 μm over the target area; this accounts for the magenta curve sometimes falling above the purple curve of constant substrate thickness.

an adjustment for 1700 nm photons (the detector is roughly 10% less sensitive at 1700 nm). Overall, we achieve an SDE of 0.20% in our system. The calculated converted power P per unit target area A, as a function of dark photon mass, is shown in Fig. 3. This power is normalized to the time-averaged power converted by a simple mirrored surface, $P_0/A = \frac{2}{3}\epsilon^2\rho_{\rm DM}$, where $\rho_{\rm DM}$ is the local DM energy density.

Results.—Over a 180 hour exposure, the primary SNSPD registered four counts, while the reference SNSPD registered five counts. As discussed in the Supplemental Material [28], the dark count rates for the two SNSPDs are likely to be similar. Accordingly, we can estimate the dark count rate for the primary SNSPD using the reference SNSPD's counts, and set a limit on the kinetic mixing ϵ, as described in the Supplemental Material [28]. Figure 4 shows this 90% confidence limit, derived by minimizing over measurement uncertainties as described below, compared with existing bounds [38]. We assume a local DM density of 0.4 GeV cm^{-3}, with a standard truncated Maxwell-Boltzmann velocity distribution [39], and assume that the dark photon polarization direction varies randomly over timescales longer than the DM coherence time (see the Supplemental Material [28] for details).

There are several measurement uncertainties on the properties of the target, such as the layer thicknesses. To set conservative limits, we calculate the minimum signal power that is compatible with the possible range of target properties (as discussed in the Supplemental Material [28]). This procedure has a non-negligible effect, since the large substrate thickness $t_s \simeq 525 \pm 10$ μm introduces an oscillatory dependence of the signal power on the DM frequency. The time-averaged DM absorption rate per unit area, as a function of dark photon mass, is shown in Fig. 3. The thin purple curve shows the signal power for a target with coplanar, uniform layers, with the measured central value thicknesses and properties, illustrating the rapid oscillation caused by the large substrate thickness. Small variations in target properties can shift these oscillations by more than a period, introducing uncertainty in the signal power at a given DM mass. Analogously, physical variation in, e.g., the substrate thickness over the disk (slowly varying over the span of the wafer, known as total thickness variation) results in a disk-averaged conversion power that is averaged over shifted curves. Taking both of these effects into account gives the magenta curve in Fig. 3.

The calculations for Fig. 3 were carried out in 1D (using transfer matrix methods [43]), treating layers locally as infinite and uniform. As discussed above and in the Supplemental Material [28], there will be deviations from this approximation. However, these deviations will only be important if, at scales $\lesssim$ the DM coherence length (which is $\simeq$0.5 mm at the relevant DM masses), they have a greater effect than the uncertainties incorporated into the 1D calculation. As discussed in the Supplemental Material [28], measurements of the stack show that, with the exception of small defects (which were incorporated into our loss calculations above), the layer properties are uniform enough that the uncertainty in converted power is dominated by the 1D effects. Another effect is that, due to wafer curvature, the angle between the layers and the lens surface will vary over the stack, being effectively coplanar in some places but not in others. Taking the minimum over 1D configurations which include the lens and its antireflection coating (treating them as coplanar with the stack), and those which do not, does not visibly alter the magenta curve in Fig. 3—the uncertain substrate thickness is already a large effect. The misalignment between the stack and the lens will also alter the focusing of the stack-generated signal, which is taken into account by our optical collection efficiency calculations. While the antireflection coating, which is itself a series of dielectric layers (whose properties we do not know precisely), could hypothetically convert DM into a photon signal which may interfere with that from the stack, the variation in stack-lens separation over the area, and the fact that the lens and stack are separated by more than the DM coherence length, mean that the converted powers will add incoherently (this is discussed in more detail in the Supplemental Material [28]).

Figure 3 illustrates that, even using our conservative estimates, our layered target enhances the conversion rate

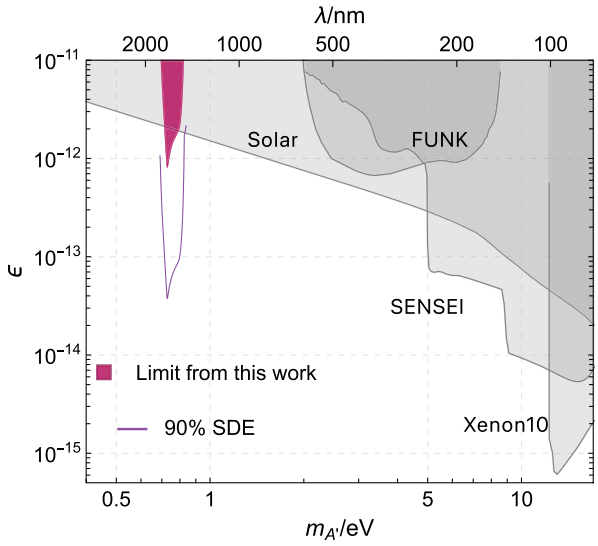

FIG. 4. LAMPOST constraints on dark photon DM with mass $m_{A'}$ and kinetic mixing ϵ. The magenta shaded region shows the 90% limit set by our experiment. The thin purple curve corresponds to the reach of an equivalent experiment with an improved SDE of 90%. Existing limits on dark photon DM from the FUNK [40], SENSEI [41], and Xenon10 [42] experiments and from the nondetection of Solar dark photons by Xenon1T [38] are shown in gray.

by up to a factor ~30 times that of a mirror target of the same area [40,44,45]. Compared with dark photon absorption in the SNSPD itself, as considered in Ref. [23], the much larger area and multiple layers of the dielectric target produce a signal rate from stack-converted photons that is at least $\sim 10^3$ times greater (at its optimum frequencies). Figure 4 shows that our prototype detector constrains previously unexplored DM parameter space in the mass range 0.7–0.8 eV.

As discussed in the Supplemental Material [28], since we do not know the precise cause of our observed counts, it is possible that the dark count rates for the reference and primary SNSPDs are somewhat different. To set a conservative limit on the kinetic mixing ϵ, we can find the value of ϵ that would lead to ≤ 4 signal counts only 10% of the time, giving a 90% confidence limit on the coupling, independent of any dark count rate estimate. This results in a ϵ limit a factor ~1.3 times larger than the nominal limit shown in Fig. 4. In future experiments, further measurements (e.g., a control experiment where the stack is removed) would enable more precise measurement of the primary SNSPD's dark count rate.

Discussion.—There are several clear directions toward extending the experimental reach beyond the prototype. The first is improving the OCE from its current value of 1.27%, which suffers from a combination of optical aberrations and reflective losses. In the future, these could be mitigated with a longer-focal length lens, reaching 93% OCE (see the Supplemental Material [28], Fig. 4), but at the expense of mechanical stability. With custom-designed adapters to house the lens, stack, and collimator, and finer toleranced parts used in the assembly, concerns over alignment could be assuaged. The other aspect would be improving the DE of the SNSPD. By adding an appropriately designed dielectric coating around the SNSPD, the DE could be raised to 98%[24]. Finally, by lowering the defect count of the target's dielectric stack, transmission losses could be made negligible. Combining these would enable a SDE above 90%, which would increase the reach of an otherwise equivalent experiment about an order of magnitude in coupling, as illustrated in Fig. 4.

Further improvement can be achieved from background count characterization and mitigation, to determine whether they originate from cosmic ray muons, Cherenkov photons generated in the lens [27], or simple statistical fluctuations of the bias current in the detector. For dark counts generated by cosmic rays or radioactivity, it may be possible to veto such events using additional detectors.

Extending the reach to heavier DM masses could be accomplished with wider-band-gap thin film materials such as ZnSe or TiO_2. To search lighter DM masses, more research should be conducted on fabricating low-energy threshold SNSPDs, though promising results have been obtained at photon energies as low as ~0.1 eV ($\lambda \sim 10\ \mu$m) [25,46].

By placing the dielectric layers in a magnetic field, axion [47–49] DM with a coupling to photons [50] could also be absorbed, allowing a haloscope to probe axion masses well above the traditional microwave range [15]. If good SNSPD performance in a large magnetic field is achieved (as has been demonstrated in some cases [51,52]), almost the same experimental setup could be used. Finally, we note that another experimental search for dark photon dark matter with a multilayer dielectric haloscope was recently published in Ref. [53].

The LAMPOST prototype places the first constraints on dark matter using optical haloscopes, exceeding current constraints in the 0.7–0.8 eV mass range by up to a factor of 2 in dark photon coupling. At the same time, the prototype demonstrates technologies and techniques that will enable searches over even larger volumes of parameter space. Optimizing the optical collection and detection efficiency of the setup can improve the coupling limits by more than an order of magnitude. Larger volumes of layered dielectric targets, longer integration times, parallel operation of complementary frequency haloscopes, and background characterization and vetoes are all concrete avenues toward a rapid exploration of large regions of dark photon dark matter parameter space. Integration with a large background magnetic field and lower-threshold SNSPDs will enable the search for axion dark matter in the meV mass range.

R. L.'s research is supported in part by the National Science Foundation under Grant No. PHYS-2014215, and the Gordon and Betty Moore Foundation, Grant No. GBMF7946. Some of the computing for this project

was performed on the Sherlock cluster at Stanford. We would like to thank Stanford University and the Stanford Research Computing Center for providing computational resources and support that contributed to these research results. We thank Dr. J. Hilfiker of J.A. Woollam Corp. for providing VASE measurements. We thank Daniel Egana-Ugrinovic, Rouven Essig, Alexander Millar, Kent Irwin, and Saptarshi Chaudhuri for useful comments and discussions. Research at Perimeter Institute is supported in part by the Government of Canada through the Department of Innovation, Science and Economic Development Canada and by the Province of Ontario through the Ministry of Colleges and Universities. The MIT coauthors acknowledge support for the later stages of the work from the Fermi Research Alliance, LLC (FRA) and the U.S. Department of Energy (DOE) under Contract No. DE-AC02-07CH11359. The initial stages of the work were supported by the DOE under the QuantiSED program, Award No. DE-SC0019129. M. B. is supported by the U.S. Department of Energy, Office of Science, Office of Basic Energy Sciences Energy Frontier Research Centers program under Award No. DE-SC0022348 and through the Department of Physics and College of Arts and Science at the University of Washington. The MIT coauthors also thank Brenden Butters for the technical work.

*jeffrey.chiles@nist.gov
†charaev@mit.edu.
‡These authors contributed equally to this work.

[1] V. C. Rubin and W. K. Ford, Jr., Astrophys. J. **159**, 379 (1970).
[2] N. Aghanim *et al.* (Planck Collaboration), Astron. Astrophys. **641**, A6 (2020).
[3] M. Dine and W. Fischler, Phys. Lett. **120B**, 137 (1983).
[4] L. F. Abbott and P. Sikivie, Phys. Lett. **120B**, 133 (1983).
[5] J. Preskill, M. B. Wise, and F. Wilczek, Phys. Lett. **120B**, 127 (1983).
[6] P. Arias, D. Cadamuro, M. Goodsell, J. Jaeckel, J. Redondo, and A. Ringwald, J. Cosmol. Astropart. Phys. 06 (2012) 013.
[7] P. W. Graham, J. Mardon, and S. Rajendran, Phys. Rev. D **93**, 103520 (2016).
[8] P. Svrcek and E. Witten, J. High Energy Phys. 06 (2006) 051.
[9] A. Arvanitaki, S. Dimopoulos, S. Dubovsky, N. Kaloper, and J. March-Russell, Phys. Rev. D **81**, 123530 (2010).
[10] B. Holdom, Phys. Lett. **166B**, 196 (1986).
[11] M. Cicoli, M. Goodsell, J. Jaeckel, and A. Ringwald, J. High Energy Phys. 07 (2011) 114.
[12] S. Dimopoulos and G. F. Giudice, Phys. Lett. B **379**, 105 (1996).
[13] T. Damour and A. M. Polyakov, Nucl. Phys. **B423**, 532 (1994).
[14] Y. Akrami *et al.* (Planck Collaboration), Astron. Astrophys. **641**, A10 (2020).
[15] M. Baryakhtar, J. Huang, and R. Lasenby, Phys. Rev. D **98**, 035006 (2018).
[16] A. Arvanitaki, S. Dimopoulos, and K. Van Tilburg, Phys. Rev. X **8**, 041001 (2018).
[17] M. W. Goodman and E. Witten, Phys. Rev. D **31**, 3059 (1985).
[18] A. Caldwell, G. Dvali, B. Majorovits, A. Millar, G. Raffelt, J. Redondo, O. Reimann, F. Simon, and F. Steffen (MADMAX Working Group), Phys. Rev. Lett. **118**, 091801 (2017).
[19] G. Carosi, R. Cervantes, S. Kimes, P. Mohapatra, R. Ottens, and G. Rybka, in *Microwave Cavities and Detectors for Axion Research*, edited by G. Carosi and G. Rybka (Springer International Publishing, Cham, 2020), pp. 169–175.
[20] B. Phillips, in *Proceedings of the 2nd Workshop on Microwave Cavities and Detectors for Axion Research, Lawrence Livermore National Laboratory* (2017).
[21] J. Sloan, in *Proceedings of the 1st Workshop on Microwave Cavity Design for Axion Detection, Livermore Valley Open Campus* (2015).
[22] M. Baryakhtar, J. Huang, and R. Lasenby, Phys. Rev. D **98**, 035006 (2018).
[23] Y. Hochberg, I. Charaev, S.-W. Nam, V. Verma, M. Colangelo, and K. K. Berggren, Phys. Rev. Lett. **123**, 151802 (2019).
[24] D. V. Reddy, R. R. Nerem, S. W. Nam, R. P. Mirin, and V. B. Verma, Optica **7**, 1649 (2020).
[25] V. B. Verma *et al.*, APL Photonics **6**, 056101 (2021).
[26] E. E. Wollman, V. B. Verma, A. D. Beyer, R. M. Briggs, B. Korzh, J. P. Allmaras, F. Marsili, A. E. Lita, R. P. Mirin, S. W. Nam, and M. D. Shaw, Opt. Express **25**, 26792 (2017).
[27] P. Du, D. Egana-Ugrinovic, R. Essig, and M. Sholapurkar, Phys. Rev. X **12**, 011009 (2022).
[28] See Supplemental Material at http://link.aps.org/supplemental/10.1103/PhysRevLett.128.231802 for additional experimental and theoretical details, which includes Refs. [29–37].
[29] M. G. Moharam and T. K. Gaylord, J. Opt. Soc. Am. **71**, 811 (1981).
[30] F. L. Pedrotti, L. M. Pedrotti, and L. S. Pedrotti, *Introduction to Optics* (Cambridge University Press, Cambridge, England, 2017).
[31] K. G. Lyon, G. L. Salinger, C. A. Swenson, and G. K. White, J. Appl. Phys. **48**, 865 (1977).
[32] T. A. Hahn and R. K. Kirby, AIP Conf. Proc. **3**, 13 (1972).
[33] Thin film mechanics, https://www.mrsec.harvard.edu/education/ap298r2004/Vlassak%20AP298presentation.pdf.
[34] G. G. Stoney and C. A. Parsons, Proc. R. Soc. A **82**, 172 (1909).
[35] Lambert's cosine law, https://en.wikipedia.org/wiki/Lambert's_cosine_law.
[36] J. Komma, C. Schwarz, G. Hofmann, D. Heinert, and R. Nawrodt, Appl. Phys. Lett. **101**, 041905 (2012).
[37] A. Caputo, A. J. Millar, C. A. J. O'Hare, and E. Vitagliano, Phys. Rev. D **104**, 095029 (2021).
[38] H. An, M. Pospelov, J. Pradler, and A. Ritz, Phys. Rev. D **102**, 115022 (2020).

[39] C. McCabe, Phys. Rev. D **82**, 023530 (2010).
[40] A. Andrianavalomahefa *et al.* (FUNK Experiment Collaboration), Phys. Rev. D **102**, 042001 (2020).
[41] L. Barak, I. M. Bloch, M. Cababie, G. Cancelo, L. Chaplinsky *et al.* (SENSEI Collaboration), Phys. Rev. Lett. **125**, 171802 (2020).
[42] J. Angle, E. Aprile, F. Arneodo, L. Baudis, A. Bernstein *et al.* (XENON10 Collaboration), Phys. Rev. Lett. **107**, 051301 (2011).
[43] A. J. Millar, G. G. Raffelt, J. Redondo, and F. D. Steffen, J. Cosmol. Astropart. Phys. 01 (2017) 061.
[44] D. Horns, J. Jaeckel, A. Lindner, A. Lobanov, J. Redondo, and A. Ringwald, J. Cosmol. Astropart. Phys. 04 (2013) 016.
[45] J. Suzuki, T. Horie, Y. Inoue, and M. Minowa, J. Cosmol. Astropart. Phys. 09 (2015) 042.
[46] F. Marsili, F. Bellei, F. Najafi, A. E. Dane, E. A. Dauler, R. J. Molnar, and K. K. Berggren, Nano Lett. **12**, 4799 (2012).
[47] S. Weinberg, Phys. Rev. Lett. **40**, 223 (1978).
[48] F. Wilczek, Phys. Rev. Lett. **40**, 279 (1978).
[49] R. D. Peccei and H. R. Quinn, Phys. Rev. Lett. **38**, 1440 (1977).
[50] P. W. Graham, I. G. Irastorza, S. K. Lamoreaux, A. Lindner, and K. A. van Bibber, Annu. Rev. Nucl. Part. Sci. **65**, 485 (2015).
[51] T. Polakovic, W. Armstrong, V. Yefremenko, J. Pearson, K. Hafidi, G. Karapetrov, Z.-E. Meziani, and V. Novosad, Nucl. Instrum. Methods Phys. Res., Sect. A **959**, 163543 (2020).
[52] B. J. Lawrie, C. E. Marvinney, Y.-Y. Pai, M. A. Feldman, J. Zhang, A. J. Miller, C. Hua, E. Dumitrescu, and G. B. Halász, Phys. Rev. Applied **16**, 064059 (2021).
[53] L. Manenti *et al.*, Phys. Rev. D **105**, 052010 (2022).

Correction: Reference [53] and its citation in the penultimate paragraph were missing and have been inserted.

Second Correction: A missing support statement has been added to the Acknowledgments section.